JACC: CARDIOVASCULAR IMAGING VOL. 6, NO. 4, 2013

ISSN 1936-878X/$36.00

PUBLISHED BY ELSEVIER INC.

http://dx.doi.org/10.1016/j.jcmg.2012.08.019

Native T1 Mapping in Differentiation of Normal Myocardium From Diffuse Disease in Hypertrophic and Dilated Cardiomyopathy

Valentina O. Puntmann, MD, PhD,* Tobias Voigt, PhD,† Zhong Chen, MD,* Manuel Mayr, MD, PhD,‡ Rashed Karim, PhD,* Kawal Rhode, PhD,* Ana Pastor, MD,* Gerald Carr-White, MBBS, PhD,* Reza Razavi, MD,* Tobias Schaeffter, PhD,* Eike Nagel, MD, PhD*

London, United Kingdom

OBJECTIVES The aim of this study was to examine the value of native and post-contrast T1 relaxation in the differentiation between healthy and diffusely diseased myocardium in 2 model conditions, hypertrophic cardiomyopathy and nonischemic dilated cardiomyopathy.

BACKGROUND T1 mapping has been proposed as potentially valuable in the quantitative assessment of diffuse myocardial fibrosis, but no studies to date have systematically evaluated its role in the differentiation of healthy myocardium from diffuse disease in a clinical setting.

METHODS Consecutive subjects undergoing routine clinical cardiac magnetic resonance at King's College London were invited to participate in this study. Groups were based on cardiac magnetic resonance findings and consisted of subjects with known hypertrophic cardiomyopathy (n = 25) and nonischemic dilated cardiomyopathy (n = 27). Thirty normotensive subjects with low pre-test likelihood of cardiomyopathy, not taking any regular medications and with normal cardiac magnetic resonance findings including normal left ventricular mass indexes, served as controls. Single equatorial short-axis slice T1 mapping was performed using a 3-T scanner before and at 10, 20, and 30 minutes after the administration of 0.2 mmol/kg of gadobutrol. T1 values were quantified within the septal myocardium ($T1_{native}$), and extracellular volume fractions (ECV) were calculated.

RESULTS $T1_{native}$ was significantly longer in patients with cardiomyopathy compared with control subjects ($p < 0.01$). Conversely, post-contrast T1 values were significantly shorter in patients with cardiomyopathy at all time points ($p < 0.01$). ECV was significantly higher in patients with cardiomyopathy compared with controls at all time points ($p < 0.01$). Multivariate binary logistic regression revealed that $T1_{native}$ could differentiate between healthy and diseased myocardium with sensitivity of 100%, specificity of 96%, and diagnostic accuracy of 98% (area under the curve 0.99; 95% confidence interval: 0.96 to 1.00; $p < 0.001$), whereas post-contrast T1 values and ECV showed lower discriminatory performance.

CONCLUSIONS This study demonstrates that native and post-contrast T1 values provide indexes with high diagnostic accuracy for the discrimination of normal and diffusely diseased myocardium. (J Am Coll Cardiol Img 2013;6:475–84) © 2013 by the American College of Cardiology Foundation

From the *Department of Cardiovascular Imaging, King's College London, London, United Kingdom; †Philips Innovative Technologies, Clinical Research, London, United Kingdom; and the ‡Cardiovascular Division, King's College London, London, United Kingdom. This study was funded by the Department of Health via the National Institute for Health Research comprehensive Biomedical Research Centre award to Guy's & St. Thomas' NHS Foundation Trust in partnership with King's College London and King's College Hospital NHS Foundation Trust. Dr. Schaeffter has received research support from Philips Healthcare. All other authors have reported that they have no relationships relevant to the contents of this paper to disclose.

Manuscript received July 3, 2012; revised manuscript received August 6, 2012, accepted August 9, 2012.

JACC: CARDIOVASCULAR IMAGING, VOL. 6, NO. 4, 2013
APRIL 2013:475–84

Myocardial fibrosis is a fundamental process in the development of myocardial dysfunction in various cardiomyopathies, leading to myocardial remodeling and poor outcomes (1–5). Cardiac magnetic resonance (CMR) is increasingly applied as the first-line investigation into the causes of cardiomyopathies (6). Visualization of fibrosis by CMR is based on a greater distribution volume and slower washout of gadolinium contrast agents within tissues with greater extracellular space due to edema or fibrosis (7). Whereas regional fibrosis after ischemic injury is readily distinguished by well-delineated areas of increased signal intensity on T1-weighted images by late gadolinium enhancement (LGE) (8), it may be impossible to define an area of clearly unaffected myocardium as a "nulled" reference in diffuse fibrotic processes (Figs. 1A and 1B) (9). As a consequence, such images may null the signal in areas of fibrosis, obscuring the finding or result in images with various gray values, not allowing a clear "yes or no" decision (9,10). Recently, several studies have proposed the measurement of T1 relaxation as potentially valuable for the quantitative assessment of myocardial fibrosis (11–16). In these studies, native myocardium with ischemic scar showed longer T1 values compared with unaffected remote myocardium. After contrast administration, regional and also diffusely scarred myocardium showed shorter T1 relaxation and delayed normalization of T1 times with gadolinium washout. Whereas these observations show the potential of T1 mapping for the evaluation of myocardial fibrosis, these studies used a variety of imaging methodologies and post-processing approaches. The ability of T1 mapping to differentiate between normal and abnormal myocardium is yet to yield a clinically robust application. In the present study, we aimed to examine the value of native and post-contrast T1 relaxation in the differentiation of healthy and diffusely diseased myocardium in 2 model conditions, hypertrophic cardiomyopathy (HCM) and nonischemic dilated cardiomyopathy (NIDCM).

See page 485

ABBREVIATIONS AND ACRONYMS

CI = confidence interval

CMR = cardiac magnetic resonance

HCM = hypertrophic cardiomyopathy

HR = heart rate

LGE = late gadolinium enhancement

LV = left ventricular

NIDCM = nonischemic dilated cardiomyopathy

ROI = region of interest

METHODS

Consecutive subjects undergoing routine clinical CMR at King's College London were invited to participate in this study. Groups were based on CMR findings and consisted of subjects with known HCM (n = 25) and NIDCM (n = 27) and controls (n = 30). Diagnosis of HCM was based on the demonstration of a hypertrophied left ventricle associated with a nondilated left ventricle (LV) in the absence of increased LV wall stress or another cardiac or systemic disease that could result in a similar magnitude of hypertrophy (17,18). All patients with HCM had an expressed phenotype with typically asymmetric septal hypertrophy of increased LV wall thickness, permitting unequivocal clinical diagnoses. NIDCM was defined as an increase in LV volumes, a reduction in global systolic function, and absence of evidence of ischemic-like LGE (18). Thirty normotensive subjects with low pre-test likelihood for LV cardiomyopathy, not taking any regular medications and, consequently, with normal CMR findings including normal LV mass indexes, served as the control group (19). Additional exclusion criteria for all subjects were the generally accepted contraindications to CMR (implantable devices, cerebral aneurysm clips, cochlear implants, severe claustrophobia) or a history of renal disease with a current estimated glomerular filtration rate <30 ml/min/1.73 m^2. The study protocol was reviewed and approved by the institutional ethics committee, and written informed consent was obtained from all participants.

CMR protocol. We integrated native and post-contrast myocardial T1 mapping into our routine imaging protocol for the determination of the underlying etiology of cardiomyopathy; an outline is provided in Figure 2. The CMR studies were performed with the patient supine, using a clinical 3-T scanner (Achieva TX, Philips Healthcare, Best, the Netherlands) and a 32-channel coil. After standardized patient-specific planning (20), volumetric cavity assessment was obtained by whole-heart coverage of gapless short-axis slices. Thereafter, cine images of 3 long-axis views (4-chamber, 2-chamber, and 3-chamber views) and transverse axial views were acquired. All cine-images were acquired using a balanced steady-state free precession sequence in combination with parallel imaging (SENSitivity Encoding, factor 2) and retrospective gating during a gentle expiratory breath-hold (echo time [TE]/repetition time [TR]/flip-angle: 1.7 ms/3.4 ms/60°, spatial resolution 1.8 × 1.8 × 8 mm). LGE imaging was performed in a gapless whole heart coverage of short axis slices 20 min after administration of a cumulative dose of 0.2 mmol/kg body weight gadobutrol using a mid-diastolic inversion prepared 2-dimensional gradient echo sequence (TE/TR/flip-angle 2.0 ms/3.4 ms/25°, interpolated voxel size 0.7 ×

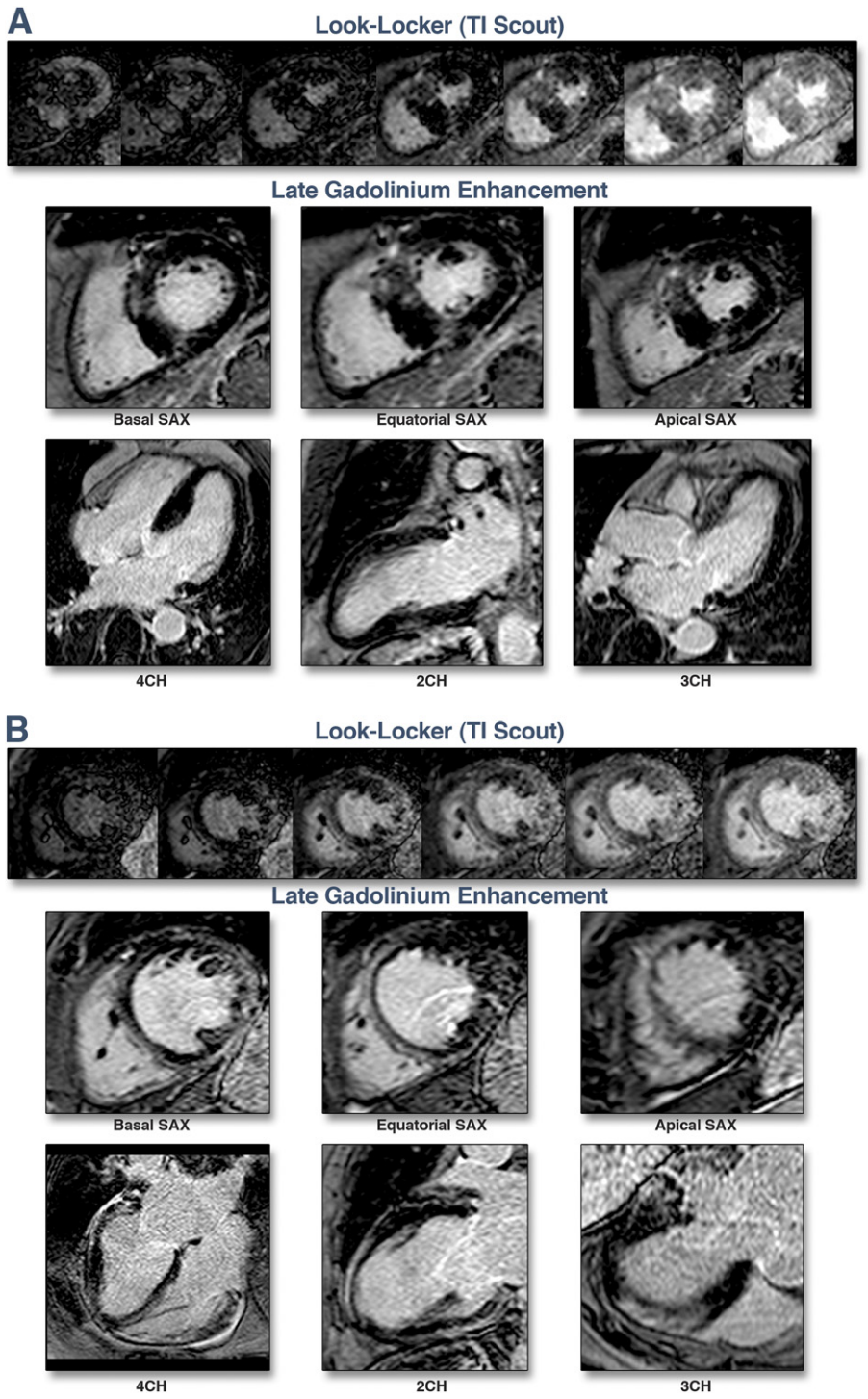

Figure 1. Examples of LGE Images in Conditions With Diffuse Myocardial Involvement

Look-Locker images and late gadolinium enhancement (LGE) images in burnt-out hypertrophic cardiomyopathy **(A)** and dilated cardiomyopathy after previous myocarditis **(B)**. There was a reduced overall relative difference in signal between affected and unaffected myocardium in Look-Locker images, leading to difficulty in nulling of the normal myocardium. 4CH = 4-chamber; SAX = short-axis; 3CH = 3-chamber; 2CH = 2-chamber.

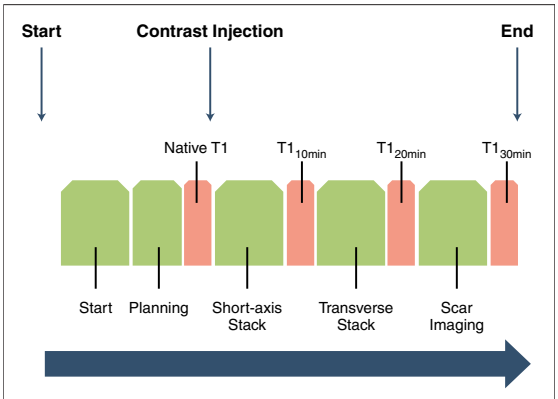

Figure 2. Integration of MOLLI Sequences in Clinical Routine

Modified Look-Locker inversion recovery (MOLLI) sequences were integrated into the clinical protocol for the investigation of cardiomyopathy, with set spacing between the time points. Time points denote the interval from gadolinium contrast administration.

0.7 × 8 mm, and a patient-adapted prepulse delay, as appropriate. A steady-state free precession, single-breath-hold modified Look-Locker inversion recovery sequence was used for T1 mapping, performed in an equatorial short-axis slice before and at 10, 20, and 30 min after contrast administration. Imaging parameters were as follows: field of view 320 × 320, TR 3.3 ms, TE 1.57 ms, flip angle 50°, interpolated voxel size 0.9 × 0.9 × 8 mm, 166 phase-encoding steps, heart rate (HR)–adapted trigger delay, 11 phases (3 + 3 + 5), and adiabatic pre-pulse to achieve a complete inversion (14–16).

Image analysis. All routine CMR analysis was performed using commercially available software (View-Forum, Extended Workspace, Philips Healthcare). Endocardial LV borders were manually traced at end-diastole and end-systole. The papillary muscles were included as part of the LV cavity volume. LV end-diastolic and end-systolic volumes were determined using Simpson's rule. Ejection fraction was computed as end-diastolic volume − end-systolic volume/end-diastolic volume. All volumetric indexes were normalized to body surface area.

The LGE images were visually examined for the presence of regional fibrosis. Global enhancement was defined as percent of enhanced area per total short-axis stack, where enhanced area was defined by 6 SDs above the manually selected normal area, appearing as maximally suppressed myocardium (10).

T1 relaxation maps were obtained using Relax-Maps tools supported by the PRIDE environment (Philips Healthcare). Selective acquisition at a fixed point of the cardiac cycle in end-diastole largely suppressed the influence of cardiac motion, but the relatively long duration of the sequence (17 heartbeats to obtain a single slice map) occasionally led to some undesired breathing motion. We therefore performed a motion correction image preparation step using a custom-made tool developed in house on the basis of a hierarchical adaptive local affine registration technique, as previously described (21), in which a reference phase (source) is registered to each of the selected target phases (11 in total). A rectangular region of interest (ROI) large enough to enclose the whole of the LV is manually drawn onto the source reference phase before registration. After the initial image affine registration step of the ROI, the source image is subdivided into 4 smaller ROIs using equal subdivisions. Each subdivision underwent an affine transformation again (each with 6 degrees of freedom) to align the features of the target image ROIs with the corresponding ROIs in the source phase image. Coregistered images were then used to derive T1 values. Because previous studies showed substantial segmental variation in T1 values, which was greatest in lateral and smallest in the septal segments (15,16), an interobserver consensus was reached to place the ROIs within the septal myocardium (Figs. 3 and 4). Care was also taken to avoid "contamination" with signal from the blood pool. Reported T1 values were derived blinded to the LGE images to enable high interobserver and intraobserver reproducibility of T1 measurements. We additionally examined the influence of visualized LGE on the T1 values, regionally

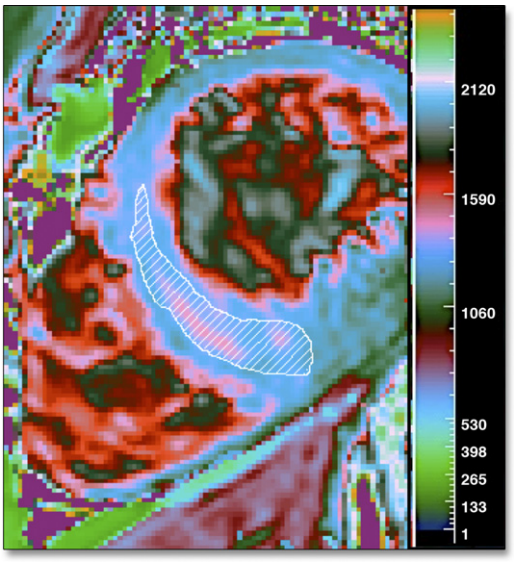

Figure 3. T1 Map With Color Scale and Region of Interest

With interobserver consensus, the region of interest was placed conservatively within the septal myocardium. Care was also taken to avoid "contamination" with signal from the blood pool.

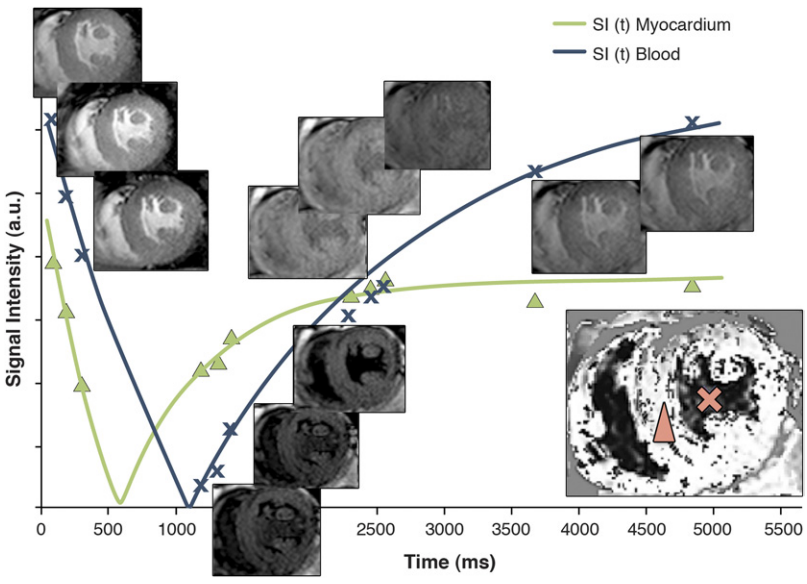

Figure 4. Representative Images of Modified Look-Locker Inversion Recovery Imaging

The region of interest was placed conservatively within the septal myocardium to avoid "contamination" with signal from the blood pool. Blood T1 values were obtained by placing the region of interest in the center of the ventricular lumen. SI = signal intensity.

and within the septal ROIs. T1 was determined by fitting a 3-parameter exponential model to the measured data and applying Look-Locker correction, as previously described (14). Noise was calculated in an ROI drawn manually inside the lungs and taken into account in the T1 computation (22). Because longitudinal relaxation is HR dependent, we also applied HR correction of T1 values when HR exceeded 80 beats/min, as previously described (14,16). In addition to the T1 values of myocardium and blood pool, we calculated volume fraction of extravascular extracellular matrix (ECV) according to the formula (22–25) ECV = [lambda × (1 − hematocrit)], where ECV is the myocardial extravascular extracellular volume fraction, and lambda = [ΔR1myocardium]/[ΔR1bloodpool] before and after gadolinium contrast (where R1 = 1/T1).

Statistical analysis. Statistical analysis was performed using SPSS version 20 (SPSS, Inc., Chicago, Illinois). Differences from the control group and between the groups were examined using one-way and repeated-measures analysis of variance with Bonferroni post hoc tests, as appropriate. Reproducibility and agreement analysis was performed using paired Student *t* tests and bivariate correlations. Associations with demographic and hemodynamic variables were detected by bivariate linear regression analyses. Multivariate binary logistic regression was used to test the ability of T1-derived measures in discrimination between healthy and abnormal myocardium. The sensitivity, specificity, and diagnostic accuracy, areas under the curve, and cutoff values were derived using receiver-operating characteristic curve analysis using the point that maximized the trade-off between specificity and sensitivity. *Z*-scores were used to compare the areas under the curve. All tests were 2 tailed, and p values <0.05 were considered significant.

RESULTS

Patients' characteristics, hemodynamic variables, and cardiac function are presented in Table 1. All groups had similar sex representations, HRs, and body surface areas. In comparison with controls, patients with HCM had increased global systolic function and diastolic LV wall thickness ($p < 0.01$). Compared with controls, subjects with NIDCM had increased cavity volumes and reduced global systolic function ($p < 0.01$). Both patient groups had increased LV mass index ($p < 0.01$). Eighteen patients with HCM and 9 with NIDCM had evidence of LGE on scar imaging, as patchy LGE or intramyocardial stria.

T1 of myocardium and blood pool and ECV. T1 values of blood pool were similar between the groups. T1 of native myocardium ($T1_{native}$) was significantly longer in cardiomyopathies compared with control subjects ($p < 0.01$) (Table 2). Conversely, post-contrast T1 values were significantly shorter in the

JACC: CARDIOVASCULAR IMAGING, VOL. 6, NO. 4, 2013
APRIL 2013:475–84

Table 1. Patient Characteristics and Global Morphological and Functional Measures

	Controls (n = 30)	Patients With HCM (n = 25)	Patients With NIDCM (n = 27)
Men	19 (63)	16 (64)	18 (67)
Age, yrs	43 ± 9	44 ± 11	45 ± 14
Systolic BP, mm Hg	113 ± 6	115 ± 6	120 ± 6
Diastolic BP, mm Hg	69 ± 8	72 ± 6	75 ± 10
HR, beats/min	64 ± 10	66 ± 9	66 ± 9
Body mass index, kg/m^2	24 ± 3	24 ± 3	23 ± 4
LVEDV index, ml/m^2	76 ± 9	70 ± 10	110 ± 15*
LV ejection fraction, %	63 ± 6	72 ± 8†	34 ± 6*
LV mass index, g/m^2	55 ± 8	99 ± 10*	106 ± 11*
Maximal LVWT, mm	9 ± 2	18 ± 2*	10 ± 2
Global enhancement, %	6 ± 5	12 ± 11*	10 ± 8†
eGFR, ml/min/1.73 m^2	82 ± 10	83 ± 9	74 ± 12
Hematocrit, %	44 ± 3	43 ± 3	43 ± 2

Values are n (%) or mean ± SD. *p < 0.01 (Bonferroni post-hoc tests for differences from the control group) and †p < 0.05.
BP = blood pressure; eGFR = estimated glomerular filtration rate; HCM = hypertrophic cardiomyopathy; HR = heart rate; LV = left ventricular; LVEDV = left ventricular end-diastolic volume; LVWT = left ventricular wall thickness; NIDCM = nonischemic dilated cardiomyopathy.

presence of cardiomyopathy at all time points (p < 0.01). Similarly, lambda values were significantly higher in patients with cardiomyopathy in comparison with controls (p < 0.01). ECV values were similar at all time points for the total cohort (10 vs. 20 vs. 30 min: 28 ± 11 vs. 29 ± 10 [p = 0.35] vs. 27 ± 9 [p = 0.22]). ECV in patients was significantly higher compared with controls at all time points (p < 0.01).

There were no significant differences in mean T1 values between subjects with visually detectable LGE and those without it ($T1_{native}$: HCM, 1,241 ± 51 ms vs. 1,234 ± 71 ms, p = 0.88, NIDCM, 1,290 ± 52 ms vs. 1,301 ± 49 ms, p = 0.58; $T1_{20min}$: HCM, 367 ± 42 ms vs. 361 ± 39 ms, p = 0.91, NIDCM, 346 ± 43 ms vs. 358 ± 48 ms, p = 0.60). Regions of visualized LGE showed no significant difference from the septal ROI T1 values for $T1_{native}$ and $T1_{20min}$ maps ($T1_{native}$ septal ROI vs. regional ROI mean difference −2.7 ± 9.4, p = 0.91; $T1_{20min}$ mean difference −1.9 ± 13, p = 0.92).

Reproducibility and agreement analysis. In a subset of subjects (n = 47), interobserver mean differences for T1 values were 1.3 ms (95% confidence interval [CI]: −12.4 to 15.4 ms) for native scans and 0.7 ms (95% CI: −7.9 to 12.3 ms) for overall post-contrast scans, whereas intraobserver mean differences were 0.3 ms (95% CI: −6.3 to −5.3) and 0.1 ms (95% CI: −3.4 to 4.2), respectively. We demonstrate

Table 2. Native and Post-Contrast T1 Relaxation Times

	Controls (n = 30)	Patients With HCM (n = 25)	Patients With NIDCM (n = 27)
Native			
T1 myocardium, ms	1,070 ± 55	1,254 ± 43*	1,239 ± 57*
T1 blood, ms	1,871 ± 89	1,869 ± 92	1,901 ± 92
R1 myocardium, ms^{-1} × 10^5	94 ± 4	80 ± 4*	76 ± 4*
10 min			
T1 myocardium, ms	402 ± 58	307 ± 47*	296 ± 43*
T1 blood, ms	247 ± 34	251 ± 39	245 ± 38
R1 myocardium, ms^{-1} × 10^5	254 ± 40	339 ± 44*	345 ± 41*
Lambda	0.46 ± 0.13	0.72 ± 0.18*	0.70 ± 0.18*
ECV	0.27 ± 0.1	0.40 ± 0.1*	0.41 ± 0.1*
20 min			
T1 myocardium, ms	440 ± 58	363 ± 63*	355 ± 44*
T1 blood, ms	294 ± 32	299 ± 36	297 ± 33
R1 myocardium, ms^{-1} × 10^5	230 ± 31	284 ± 50*	284 ± 30*
Lambda	0.49 ± 0.12	0.73 ± 0.2*	0.73 ± 0.09*
ECV	0.27 ± 0.09	0.41 ± 0.12*	0.40 ± 0.09*
30 min			
T1 myocardium, ms	504 ± 38	437 ± 49†	444 ± 45†
T1 blood, ms	381 ± 42	369 ± 37	351 ± 45
R1 myocardium, ms^{-1} × 10^5	199 ± 14	230 ± 20*	227 ± 23*
Lambda	0.47 ± 0.09	0.67 ± 0.10*	0.67 ± 0.12*
ECV	0.26 ± 0.07	0.38 ± 0.11*	0.38 ± 0.1*

*p < 0.01 (Bonferroni post-hoc tests for differences from the control group) and †p < 0.05.
ECV = extracellular volume; other abbreviations as in Table 1.

Table 3. Results of Cutoff Values on Receiver-Operating Characteristic Curve Analysis

	Cutoff Value	AUC (95% CI)	Significance (p Value)	Specificity (%) (95% CI)	Sensitivity (%) (95% CI)	Diagnostic Accuracy (%) (95% CI)
T1 value, ms						
Native	1,184	0.99 (0.98–1.00)	0.000	97 (82–100)	100 (90–100)	99 (91–99)
10 min	330	0.90 (0.87–0.97)	0.000	71 (52–85)	86 (72–94)	80 (68–88)
20 min	407	0.86 (0.79–0.96)	0.000	71 (52–85)	82 (67–92)	77(65–86)
30 min	477	0.84 (0.74–0.96)	0.000	68 (49–83)	71 (59–87)	70 (57–79)
ECV						
ECV_{10min}	23	0.86 (0.76–0.95)	0.000	70 (48–85)	80 (65–90)	78 (63–86)
ECV_{20min}	23	0.85 (0.77–0.95)	0.000	72 (50–87)	82 (66–92)	78 (65–87)
ECV_{30min}	23	0.88 (0.80–0.96)	0.000	68 (46–85)	82 (64–90)	77 (64–86)

AUC = area under the curve; CI = confidence interval; other abbreviations as in Table 2.

excellent overall (pre-contrast and post-contrast) intraobserver and interobserver agreement in T1 values (intraobserver: $r = 0.99$, $p < 0.0001$; interobserver: $r = 0.98$, $p < 0.0001$).

Comparisons of T1 measures in discrimination between normal and abnormal myocardium. In multivariate binary logistic regression model using native and post-contrast T1 and ECV values, we identified $T1_{native}$ as the independent discriminator of cardiomyopathic myocardium ($p = 0.001$), with sensitivity of 100%, specificity of 96%, diagnostic accuracy of 98%, a positive predictive value of 98%, and a negative predictive value of 100%. Comparison of areas under the curve showed that $T1_{native}$ provided the best distinction between controls and patients with cardiomyopathy ($T1_{native}$ vs. T_{10min}: $z = 2.2$, $p = 0.05$; $T1_{native}$ vs. ECV_{20min}: $z = 2.4$, $p < 0.02$). Results of receiver-operating characteristic curve analysis with corresponding cutoff values for the performance of separate T1-derived measures in the differentiation of normal from abnormal myocardium are presented in Table 3 and Figure 5.

Analysis of relationships. Within the separate patient groups, there was a positive association between $T1_{native}$ and ECV and age ($T1_{native}$: $r = 0.53$, $p = 0.03$; ECV: $r = 0.51$, $p < 0.05$). In controls and patients with NIDCM, myocardial $T1_{native}$ showed negative associations with indexed LV end-diastolic volume ($r = 0.37$ and 0.54, respectively, $p < 0.05$). Patients with NIDCM showed further associations between myocardial $T1_{native}$ and ejection fraction ($r = -0.61$, $p < 0.01$), whereas in patients with HCM, there was a positive association between myocardial $T1_{native}$ and indexed LV mass ($r = 0.51$, $p < 0.01$).

DISCUSSION

Our study reveals that diffusely diseased myocardium can be reliably differentiated from healthy myocardium by means of T1 mapping. We demonstrate that in HCM and NIDCM, native and post-contrast T1 values provide indexes with high diagnostic accuracy, sensitivity, and specificity, with $T1_{native}$ providing the greatest distinction between healthy and diffusely diseased myocardium. We further demonstrate that in NIDCM, $T1_{native}$ correlates with measures of LV remodeling and global systolic function, whereas in HCM, it shows an association with indexed LV mass. Our findings provide a novel and easy-to-use method for the detection of diffusely diseased myocardial tissue by CMR with an immediate potential for clinical translation.

T1 mapping techniques provide quantifiable information on longitudinal relaxation through the

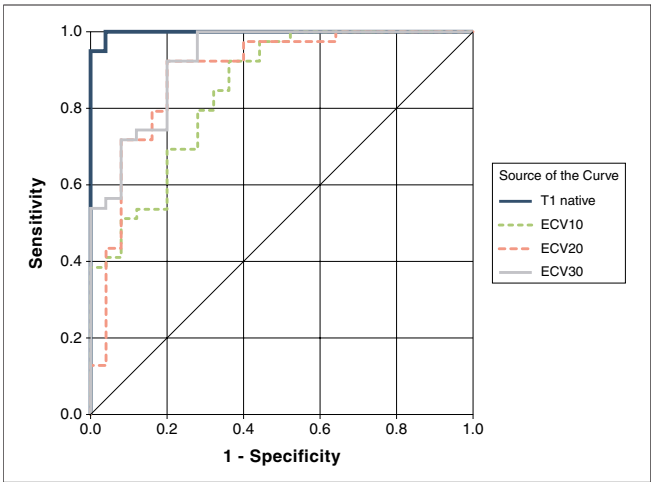

Figure 5. ROC Curves for T1-Derived Values in Differentiation Between Healthy and Abnormal Myocardium

Receiver-operating characteristic (ROC) curve analysis for the performance of separate T1-derived measures in the differentiation of normal from abnormal myocardium. Myocardial $T1_{native}$ imaging provided the best distinction between controls and patients with cardiomyopathy. ECV = extracellular volume.

acquisition of images with different inversion times and by multiparametric curve-fitting analysis. T1 maps are derived as parametric reconstructed images, in which the signal intensity of a pixel depends on the absolute longitudinal relaxation properties of this voxel (13–16,22). Several methodologies were tested to acquire the myocardial T1 relaxation values, including sets of saturation or inversion recovery images (12) with varying inversion times and, lately, the classical and modified Look-Locker sequences (14–16,23). The variant of the latter sequence, which was also applied in the present study, leads to a series of multiple images acquired within the same phase of cardiac cycle through a selective fixed delay time over successive heartbeats (14). Some studies using this or related methodologies suggested that myocardial $T1_{native}$ values could be used to discern post-infarct scar from healthy myocardium (15,16). Most of these studies, however, focused on the post-contrast T1 values and reported significantly shorter T1 times compared with controls. In a population of patients with mixed causes of heart failure, Iles et al. (12) reported shorter post-contrast T1 compared with controls, even when excluding areas of regional fibrosis. These investigators also observed an inverse relationship between post-contrast T1 values and the amount of fibrosis on histology (12). The ability of T1 imaging to quantify the amount of diffuse fibrosis was also confirmed using a novel technique of ECV imaging deriving ECV using continuous infusion (24,25). Diastolic myocardial impairment, an indirect marker of diffuse myocardial fibrosis, was shown to correlate with abnormal post-contrast T1 values in patients with heart failure, diabetic cardiomyopathy, and amyloidosis (11,26–28). Whereas Iles et al. (12) showed no significant difference in myocardial $T1_{native}$ values in patients with heart failure, our findings reveal for the first time that native T1 values are significantly higher in diffusely disease myocardium, which cannot be accounted for by the presence of visualized LGE. The disparity with the former findings may lie in the differences in patient selection, as well as imaging techniques and higher field strength used in the present study, which explains higher measurements of longitudinal relaxation in native myocardium (15,16,29).

In our study, myocardial $T1_{native}$ provides the greatest distinction between healthy myocardium and diseased tissue with high negative predictive value. As such, it bears potential for the development of an easy-to-implement test in patients with suspected diffuse fibrosis, which may be missed by classic LGE imaging. Furthermore, in subjects with low pre-test likelihood for the presence of cardiomyopathy (descriptive of our control group), or those in whom contrast administration is contraindicated, it may serve as an effective screening test. Future advances in sequence development that would provide whole-heart coverage might derive a useful approach to characterize regional differences and potentially obviate the need for contrast administration.

The observed findings in myocardial $T1_{native}$ emphasize several important aspects with regard to post-contrast T1 mapping. Because gadolinium administration greatly shortens T1 values, the overall T1 tissue relaxation will depend on the dose and relaxivity of the gadolinium contrast agent, the intrinsic T1 values of the tissue (13,23,29), and the timing of the acquisition and bioavailability after gadolinium administration (7,9). Post-contrast T1 sampling can thus be affected by a variety of independent variables, including renal function, contrast type and dose of administration, variation in sampling time points, and individual pharmacokinetics (22,30). Post-contrast T1 imaging at the rigid time points can prove cumbersome in clinical routine; we improved the interstudy comparability of the post-contrast T1 sampling by using consistent time points in our routine cardiomyopathy imaging protocol. Yet the aforementioned influences might explain the lower performance of post-contrast T1 values and ECV.

In our study, T1 values were sampled in 2 model conditions of diffuse myocardial fibrosis. Whereas several investigators have looked at the role of T1 mapping in patients with heart failure, no previous study has systematically assessed native and post-contrast T1 values in patients with HCM. It is well established that visualization of LGE in HCM has important and independent prognostic implications (5), but recent evidence suggests that a profibrotic state through genetically driven collagen metabolism precedes the overt phenotype with LV hypertrophy or fibrosis visible on LGE (4). We previously demonstrated that global enhancement correlates with reduction of longitudinal ventricular deformation in HCM, even when global systolic function remains apparently unaffected (10). Whether T1-derived measures are able to detect subclinical change in collagen metabolism remains to be determined. The identification of early phenotypes in which early fibrotic process could be quantified and followed up before the effects on

cardiac geometry and function would add to the management of this condition (4).

The observed changes in post-contrast T1 values have been previously related to increase in extracellular space and well described in models of acute and chronic ischemic or inflammatory myocardial injury. The physiological correlate with diffuse myocardial pathology and observed increases in native T1 is less well understood. Extracellular matrix remodeling is orchestrated by fibroblasts within the heart, but changes in extracellular matrix composition affect cardiomyocyte survival (1–3,31). The accumulation of extracellular matrix in pathological hypertrophy or LV remodeling with increasing age and LV mass may underlie the observed increase in myocardial $T1_{native}$ values (1). Further studies are needed to elucidate the links between exact molecular mechanisms in health and disease and the corresponding $T1_{native}$ readouts.

Study limitations. The small sample size of otherwise similar groups may limit the associations with sex and age and generalization of the present findings, and a larger multicenter study is required to reconfirm our imaging protocol beyond the proof of concept for widespread clinical use. Examination of the equivalence of multivendor sequences may also be appropriate. Next, T1 sampling in the septum of a single short-axis slice is based on the assumption that it is representative of the diffuse myocardial process, but future studies with multiple slices are needed to determine and understand relevant regional variation. The prolonged acquisition time required for longitudinal relaxation to occur in the native myocardium, especially at high field strengths, its HR dependence, and motion artifacts may all amount to errors in the pixel-wise estimation of T1 values (32). Because we used motion and HR correction algorithms and a very conservative approach to T1 sampling, we believe that we controlled for the majority of these influences. Whether imaging with shorter variants of modified Look-Locker inversion recovery sequences would resolve some of the breathing motion artifacts and still provide sufficient information on longitudinal relaxation of the native myocardium remains to be confirmed in future studies. Similarly, the effects of T2 recovery when longitudinal relaxation is measured with modified Look-Locker inversion recovery remain to be determined. Whereas in the present study, we looked at 2 models of diffuse myocardial fibrosis, we assume that the presence of edema and its influence on T1 values is unlikely a relevant substrate. Lastly, T1 values in other cardiomyopathies need to be examined in future studies.

CONCLUSIONS

We demonstrate that native and post-contrast T1 values provide indexes with high diagnostic accuracy for the discrimination of normal and diffusely diseased myocardium, as observed in patients with HCM and NIDCM in the present study. Myocardial $T1_{native}$ imaging provides the best distinction between controls and patients with cardiomyopathy. Further studies are needed to effectively translate these findings into clinical use.

Acknowledgment

The authors acknowledge Lorna Smith, head of research radiography in the Department of Cardiovascular Imaging Sciences, King's College London, for her assistance with high-quality data acquisition and clinical application support.

Reprint requests and correspondence: Prof. Eike Nagel, King's College London, Department of Cardiovascular Imaging, The Rayne Institute, 4th Floor Lambeth Wing, St. Thomas' Hospital Campus, London SE1 7EH, United Kingdom. *E-mail: eike.nagel@kcl.ac.uk.*

REFERENCES

1. Hill JA, Olson EN. Cardiac plasticity. N Engl J Med 2008;358:1370–80.
2. Van den Borne SW, Diez J, Blankesteijn WM, Verjans J, Hofstra L, Narula J. Myocardial remodeling after infarction: the role of myofibroblasts. Nat Rev Cardiol 2010;7:30–7.
3. Barallobre-Barreiro J, Didangelos A, Schoendube FA, et al. Proteomics analysis of cardiac extracellular matrix remodeling in a porcine model of ischemia-reperfusion injury. Circulation 2012;125:789–802.
4. Ho CY, Lopez B, Coelho-Filho OR, et al. Myocardial fibrosis as an early manifestation of hypertrophic cardiomyopathy. N Engl J Med 2010;363:552–63.
5. Bruder O, Wagner A, Jensen CJ, et al. Myocardial scar visualized by cardiovascular magnetic resonance imaging predicts major adverse events in patients with hypertrophic cardiomyopathy. J Am Coll Cardiol 2010;56:875–87.
6. Bruder O, Schneider S, Nothnagel D, et al. EuroCMR (European Cardiovascular Magnetic Resonance) registry: results of the German pilot phase. J Am Coll Cardiol 2009;54:1457–66.
7. Rehwald WG, Fieno DS, Chen EL, Kim RJ, Judd RM. Myocardial magnetic resonance imaging contrast agent concentrations after reversible

and irreversible ischemic injury. Circulation 2002;105:224–9.

8. Kim RJ, Wu E, Rafael A, et al. The use of contrast-enhanced magnetic resonance imaging to identify reversible myocardial dysfunction. N Engl J Med 2000;343:1445–53.
9. Grebe O, Paetsch I , Kestler HA, et al. Optimal acquisition parameters for contrast enhanced magnetic resonance imaging after chronic myocardial infarction. J Cardiovasc Magn Reson 2003;4:575–87.
10. Puntmann VO, Jahnke C, Gebker R, et al. Usefulness of magnetic resonance imaging to distinguish hypertensive and hypertrophic cardiomyopathy. Am J Cardiol 2010;106:1016–22.
11. Mewton N, Liu CY, Croisille P, Bluemke D, Lima JA. Assessment of myocardial fibrosis with cardiovascular magnetic resonance. J Am Coll Cardiol 2011;57:891–903.
12. Iles L, Pfluger H, Phrommintikul A, et al. Evaluation of diffuse myocardial fibrosis in heart failure with cardiac magnetic resonance contrast-enhanced T1 mapping. J Am Coll Cardiol 2008; 52:1574–80.
13. Blume U, Lockie T, Stehning C, et al. Interleaved T(1) and T(2) relaxation time mapping for cardiac applications. J Magn Reson Imaging 2009;29:480–7.
14. Messroghli DR, Radjenovic A, Kozerke S, Higgins DM, Sivananthan MU, Ridgway JP. Modified Look-Locker inversion recovery (MOLLI) for high-resolution T1 mapping of the heart. Magn Reson Med 2004;52:141–6.
15. Messroghli DR, Walters K, Plein S, et al. Myocardial T1 mapping: application to patients with acute and chronic myocardial infarction. Magn Reson Med 2007;58:34–40.
16. Piechnik SK, Ferreira VM, Dall' Armellina E, et al. Shortened modified Look-Locker inversion recovery (ShMOLLI) for clinical myocardial T1-mapping at 1.5 and 3 T within a 9 heartbeat breathhold. J Cardiovasc Magn Reson 2010;12:69.
17. Maron BJ, McKenna WJ, Danielson GK, et al., for the American College of Cardiology Foundation Task Force on Clinical Expert Consensus Documents; European Society of Cardiology Committee for Practice Guidelines. American College of Cardiology/European Society of Cardiology clinical expert consensus document on hypertrophic cardiomyopathy. A report of the American College of Cardiology Foundation Task Force on Clinical Expert Consensus Documents and the Classification of Cardiomyopathies. European Society of Cardiology Committee for Practice Guidelines. J Am Coll Cardiol 2003;42:1687–713.
18. Elliott P, Andersson B, Arbustini E, et al. Classification of the cardiomyopathies: a position statement from the European Society of Cardiology Working Group on Myocardial and Pericardial Diseases. Eur Heart J 2008;29:270–6.
19. Natori S, Lai S, Finn JP, et al. Cardiovascular function in multi-ethnic study of atherosclerosis: normal values by age, sex, and ethnicity. AJR Am J Roentgenol 2006;186 Suppl:S357–65.
20. Kramer CM, Barkhausen J, Flamm SD, Kim RJ, Nagel E, for the Society for Cardiovascular Magnetic Resonance Board of Trustees Task Force on Standardized Protocol. Standardized cardiovascular magnetic resonance imaging (CMR) protocols, Society for Cardiovascular Magnetic Resonance: Board of Trustees Task Force on Standardized Protocols. J Cardiovasc Magn Reson 2008;10:35.
21. Buerger C, Schaeffter T, King AP. Hierarchical adaptive local affine registration for fast and robust respiratory motion estimation. Med Image Anal 2011;15:551–64.
22. Karlsen OT, Verhagen R, Bovée WMM. Parameter estimation from Rician-distributed data sets using a maximum likelihood estimator: Application to t1 and perfusion measurements. Magn Reson Med 1999;41: 614–23.
23. Schelbert EB, Testa SM, Meier CG, et al. Myocardial extravascular extracellular volume fraction measurement by gadolinium cardiovascular magnetic resonance in humans: slow infusion versus bolus. J Cardiovasc Magn Reson 2011;13:16–30.
24. Flett AS, Hayward MP, Ashworth MT, et al. Equilibrium contrast cardiovascular magnetic resonance for the measurement of diffuse myocardial fibrosis: preliminary validation in humans. Circulation 2010;122:138–44.
25. Ugander M, Oki AJ, Hsu LY, et al. Extracellular volume imaging by magnetic resonance imaging provides insights into overt and sub-clinical myocardial pathology. Eur Heart J 2012; 33:1268–78.
26. Maceira AM, Joshi J, Prasad SK, et al. Cardiovascular magnetic resonance in cardiac amyloidosis. Circulation 2005; 111:186–93.
27. Jellis C, Wright J, Kennedy D, et al. Association of imaging markers of myocardial fibrosis with metabolic and functional disturbances in early diabetic cardiomyopathy. Circ Cardiovasc Imaging 2011;4:693–702.
28. Martos R, Baugh J, Ledwidge M, et al. Diastolic heart failure: evidence of increased myocardial collagen turnover linked to diastolic dysfunction. Circulation 2007;115:888–95.
29. Sharma P, Socolow J, Patel S, Pettigrew RI, Oshinski JN. Effect of Gd-DTPA-BMA on blood and myocardial T1 at 1.5T and 3T in humans. J Magn Reson Imaging 2006;23:323–30.
30. Knowles BR, Batchelor PG, Parish V, et al. Pharmacokinetic modeling of delayed gadolinium enhancement in the myocardium. Magn Reson Med 2008;60:1524–30.
31. Anversa P, Hiler B, Ricci R, Guideri G, Olivetti G. Myocyte cell loss and myocyte hypertrophy in the aging rat heart. J Am Coll Cardiol 1986;8: 1441–8.
32. Sievers B, Rehwald WG, Albert TS, et al. Respiratory motion and cardiac arrhythmia effects on diagnostic accuracy of myocardial delayed-enhanced MR imaging in canines. Radiology 2008;247:106–14.

Key Words: diffuse fibrosis ■ hypertrophic cardiomyopathy ■ late gadolinium enhancement ■ T1 mapping.